ELSEVIER

Journal of Atmospheric and Solar-Terrestrial Physics 65 (2003) 1265 – 1282

Journal of ATMOSPHERIC AND SOLAR-TERRESTRIAL PHYSICS

www.elsevier.com/locate/jastp

Local time and longitude dependence of the equatorial electrojet magnetic effects

V. Doumouya[a,*], Y. Cohen[b], B.R. Arora[c], K. Yumoto[d]

[a] *Laboratoire de Physique de l'Atmosphère, Université de Cocody-Abidjan, 22 BP 582, Abidjan 22, Ivory Coast*

[b] *Département de Géophysique Spatiale et Planétaire, Institut de Physique du Globe de, 4, avenue de Neptune, 94107 Saint-Maur, Paris, France*

[c] *Solid Earth Geomagnetism Division, Indian Institute of Geomagnetism, Colaba, Mumbai 400005, India*

[d] *Department of Earth and Planetary Sciences, Kyushu University 33, 6-10-1 Hakozaki, Fukuoka 812-8581, Japan*

Abstract

An empirical model of the equatorial electrojet (EEJ), including local time and longitude dependence, has been constructed based on the surface magnetic data recorded at 26 stations located in six different longitude sectors that were set up or augmented during the international equatorial electrojet year (IEEY). The model reproduces the characteristic signatures of the EEJ-associated horizontal and vertical magnetic components at ground level. The model-predicted variations at the orbit of the POGS satellite are generally in good agreement with the onboard magnetic signatures, although strong discrepancies are also often seen. The nature of the differences suggests that the global scale magnetospheric or field-aligned current systems may sometimes dominate the satellite data. The nature of the longitudinal inequalities in the EEJ strength indicates that the equatorial electrojet is strongest in South America (80°–100°W) and weakest in the Indian sector (75°E) with a secondary minimum and a maximum centered, respectively, in the Atlantic Ocean (30°W) and in western Africa (10°E). The EEJ strength is shown to be inversely correlated with the main field intensity along the dip-equator.

Keywords: Equatorial electrojet; Magnetic fields; POGS satellite; Electrojet models; Longitudinal variations

1. Introduction

Since its discovery, after the installation of a geomagnetic observatory at Huancayo (Peru) near the dip-equator, the equatorial electrojet (EEJ) has been the subject of many studies. Most of the first studies were carried out to explain the generating mechanism of such an intense current flow along the dip-equator (Baker and Martyn, 1953; Chapman and Bartels, 1940). Since the 1970s, some theories and physical models of the ionospheric dynamo have been developed (Sugiura and Cain, 1966; Untiedt, 1967; Sugiura and Poros, 1969; Richmond, 1973; Stening, 1985; Reddy, 1989) in order to explain the mechanism of the EEJ flow and its main features (day to day, seasonal variability, counter-electrojet, electrodynamic processes of coupling with global scale current systems, etc). Another approach to simulate the EEJ has been through the analysis of EEJ magnetic effects assuming simple current configurations. These are the line current (Forbush and Casaverde, 1961), the thin-band current with different modes of latitudinal dependence: the uniform and parabolic (Chapman, 1951) and the "fourth degree" current distribution (Fambitakoye and Mayaud, 1976) as well as the thick current distribution incorporating latitude and height dependence (Onwumechili, 1967).

After a short standby during the late 1970s, the analysis of the Magsat data resulted in an increased interest in the

* Corresponding author. Tel.: 225-22-41-8261; fax: 225-22-44-0412.

E-mail addresses: vafid@yahoo.fr (V. Doumouya), cohen@ipgp.jussieu.fr (Y. Cohen), bra@iig.iigm.res.in (B.R. Arora), yumoto@geo.kyushu-u.ac.jp (K. Yumoto).

1364-6826/$ - see front matter
doi:10.1016/j.jastp.2003.08.014

EEJ studies (Langel et al., 1982; Yanagisawa and Kono, 1985; Cohen and Achache, 1990; Langel et al., 1993; Ravat and Hinze, 1993). The Magsat anomaly maps determined using dawn and dusk data were found to be contaminated by the EEJ signatures near the dip-equator (Maeda et al., 1982). In the frame of Magsat data analysis, different methods have been proposed to estimate or eliminate the EEJ effects: Langel et al. (1982) only averaged dawn and dusk data while Cohen and Achache (1990) obtained the EEJ effects using a mean square method. Other approaches were used for the reduction of the EEJ contribution in Magsat data (Yanagisawa and Kono, 1985; Ravat and Hinze, 1993). For non-sun-synchronous satellites (Φrsted, Champ and future geomagnetic satellites), the applications of these diverse Magsat reduction formulations should be reworded.

These significant developments from the Magsat data analysis were also taken into account in designing field experiments and subsequent analysis of the data collected during the International Equatorial Electrojet Year (IEEY). In the framework of the IEEY campaign, dense magnetometer networks were operated in Brazil (Rigoti et al., 1999), India (Arora et al., 1993) and West Africa (Amory-Mazaudier et al., 1993; Doumouya et al., 1998; Vassal et al., 1998). The main features of the EEJ, e.g. latitudinal structures and its day to day and seasonal variability, in each of the regions has been reported in the series of the papers (Arora et al., 1993; Rigoti et al., 1999; Doumouya et al., 1998). Integration of the global data collected during the IEEY gives further opportunity to study the longitudinal dependence of the EEJ on the basis of simultaneous surface measurements.

In this paper, an empirical EEJ model is developed using simultaneous surface magnetic data recorded at 26 stations in different longitude sectors (Amory-Mazaudier et al., 1993). The model, in addition to the latitudinal structure, includes terms to describe the local time and longitude dependence. Comparison of the modeled magnetic effects with ground-based and satellite magnetic measurements validates the model. The derived model parameters are used to study the longitudinal dependence of the EEJ strength. The efficacy of the model is also tested against satellite magnetic data for correction from the EEJ contamination.

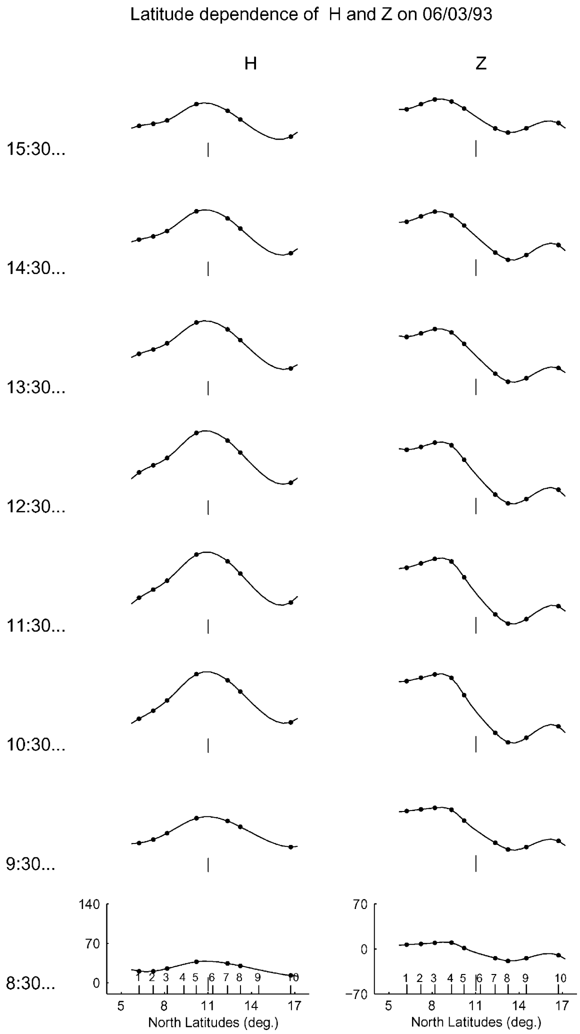

Fig. 1. Latitude dependence of the horizontal (H) and vertical (Z) components of the equatorial electrojet associated magnetic effects in West Africa. The vertical line below each curve indicates the position of the dip-equator.

2. An empirical model of the electrojet based on surface measurements

2.1. Latitudinal structure of the EEJ

Empirical models of the EEJ, based on the regular daily variation (S_R) of the Earth's magnetic field, have mostly relied on latitudinal profiles of the horizontal (ΔH) and the vertical (ΔZ) components generally reckoned with respect to the nighttime level (Fig. 1). The EEJ has been considered as a thin current ribbon flowing parallel to the dip-equator at a fixed altitude ($h = 105$ km), which was estimated from in situ rocket measurements in the equatorial ionosphere (Maynard, 1967; Sampath and Sastry, 1979). For the models that describe only the latitude dependence of the EEJ, the involved parameters are the latitude of the center (c), the peak current intensity (I_0) at the center and the half-width (a) of the EEJ. These models are particularly well suited to describe the EEJ behaviors around local noon. The well-known models can be summarized through the following formulas giving the current intensity $I(x)$ at a given latitudinal distance (x) from the equator:

- A uniform current distribution:

$$I(x) = I_0. \quad (1)$$

- A parabolic distribution after Chapman (1951):

$$I(x) = I_0\left(1 - \frac{(x-c)^2}{a^2}\right). \tag{2}$$

- And a "quadratic" or fourth degree current distribution model after Fambitakoye and Mayaud (1976):

$$I(x) = I_0\left(1 - \frac{(x-c)^2}{a^2}\right)^2. \tag{3}$$

In eqs. (1)–(3) x is defined in the range: $c - a \leqslant x \leqslant c + a$, where a is the half-width and c the position of the center of the EEJ.

Onwumechili (1992), drawing upon the limitations of these thin current models, proposed a thick current distribution model that includes both latitude and height structure. The suitability of the thin current model is determined by how well the computed model fields fit the latitudinal behavior of the observed magnetic measurements. In particular, the quadratic distribution models have been shown to fit the magnetic data from a dense network quite adequately Fambitakoye and Mayaud (1976).

The magnetic effects of the EEJ are obtained using the parameters a, c and I_{12}, derived from the latitudinal profiles of ΔH and ΔZ. Details of the computational steps to obtain a and c are given by Fambitakoye and Mayaud (1976) and Doumouya et al. (1998). I_{12} is computed from the peak value of the amplitude at noon (ΔH_{12}), derived from the latitudinal profile of ΔH at noon. The following formula, corresponding to a uniform current distribution (Fambitakoye, 1976), is used:

$$I_{12} = \frac{\Delta H_{12}}{0.4\,\mathrm{arct}g(\frac{a}{h})}, \tag{4}$$

where a is the half-width of the EEJ and is expressed (Fambitakoye, 1976) by

$$a = \sqrt{\left(\frac{d^2}{4} - h^2\right)}, \tag{5}$$

where h is the height of the EEJ , adopted as 105 km, and d is the latitudinal distance between those stations where the ΔZ variations associated with the EEJ register maximum and the minimum.

2.2. Local time dependence of the EEJ

Fig. 2 presents a typical regular daily variation in the horizontal and vertical magnetic components associated with the EEJ at ground stations spread across the dip-equator in the African sector. EEJ-related magnetic effects in the daily variations of the horizontal (ΔH) and vertical (ΔZ) components appear at about 6 LT, reach a maximum (or a minimum for ΔZ to the north of the dip-equator) near local noon and vanish after 18 LT. Fig. 3a shows the diurnal variation of the normalized ΔH^* ($\Delta H^* = (\Delta H/\Delta H_{12})$, where ΔH_{12}

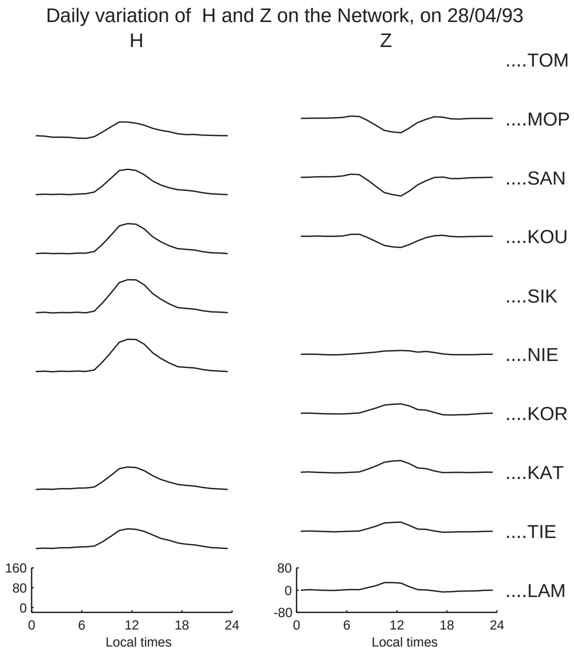

Fig. 2. The local time dependence of the horizontal (H) and vertical (Z) components of the equatorial electrojet associated magnetic effects in West Africa.

is the noon value of ΔH at the EEJ center) in West Africa (dotted curve) on February 24, April 28 and May 25, 1993. The solid curves in figure represent the local time (t) dependence of the EEJ as expressed by the Gaussian function $G(t)$, defined as follows:

$$G(t) = \exp\left(-\frac{(t-T)^2}{t_{\mathrm{m}}^2}\right). \tag{6}$$

T is the local hour of the maximum of the ΔH in the daily variation under the EEJ. On average, $T = 12$ LT with possible deviations of ± 1 h. This parameter may change from day-to-day and with season. t_{m} is a fitting parameter that controls the time window of the Gaussian-like shape of the diurnal progression in ΔH and ΔZ. It is determined by trial and error. On average, $t_{\mathrm{m}} = 4$ h for the daily variation along the West African sector. This value of t_{m} also fits the daily variations in India and in Brazil as shown in Fig. 3b and c. In general, ΔH rises more sharply in the morning and decreases more gradually in the afternoon but we notice from Figs. 3a–c that the Gaussian function $G(t)$ provides a good description of the diurnal progression. Therefore, the diurnal variation of current intensity at the center of the EEJ can be equivalently expressed as

$$I_0(t) = I_{12}\exp\left(-\frac{(t-T)^2}{t_{\mathrm{m}}^2}\right), \tag{7}$$

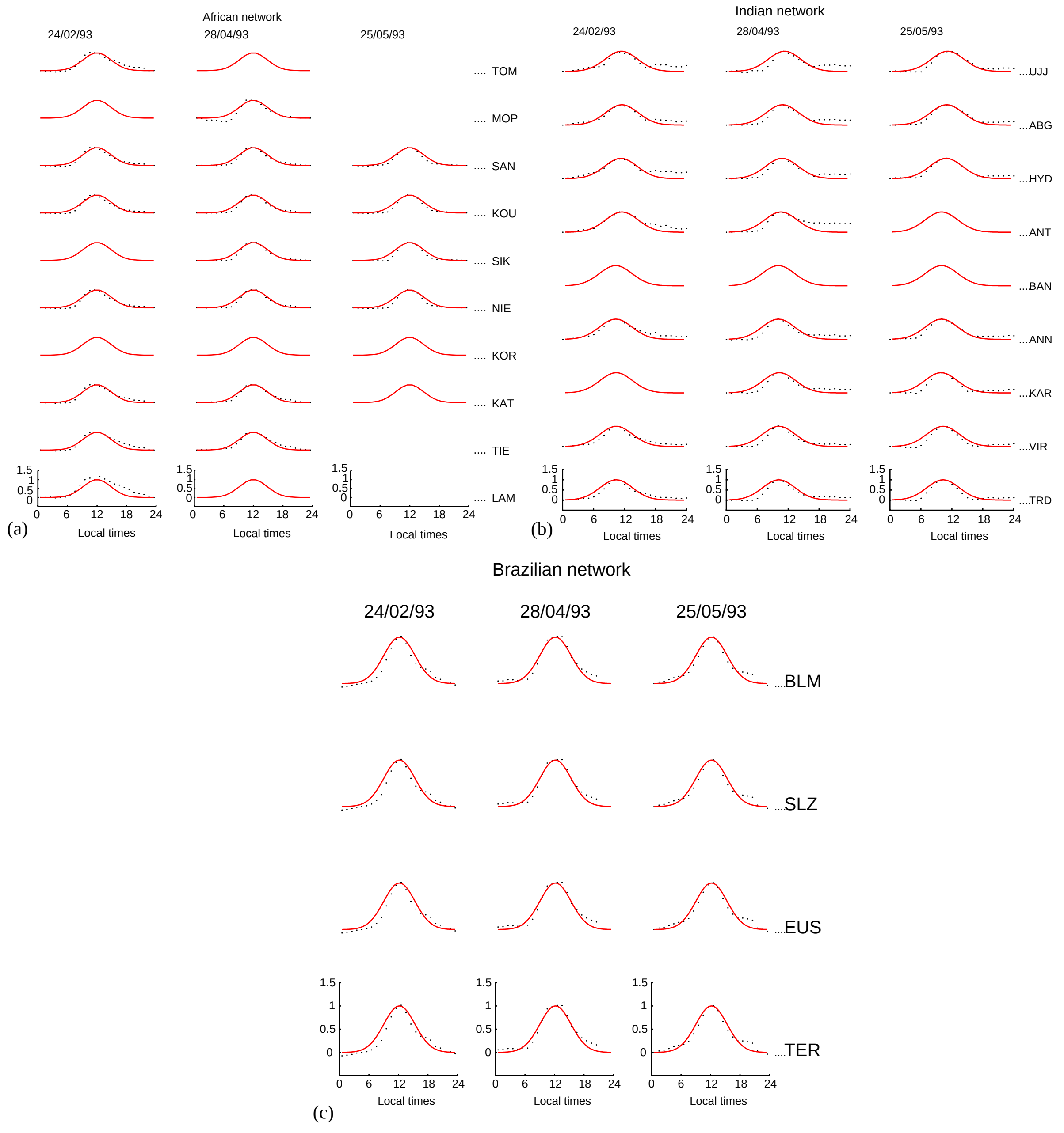

Fig. 3. (a) Comparison between a Gaussian function (solid lines) and the normalized ΔH^* ($\Delta H^* = (\Delta H/\Delta H_{12})$) daily variation of the EEJ magnetic effects (dotted line) in West Africa during the IEEY; (b) a Gaussian (solid lines) fit to the normalized ΔH^* daily variation of the EEJ magnetic effects (dotted line) along Indian longitude sector during the IEEY; (c) a Gaussian (solid lines) fit to the normalized ΔH^* daily variation of the EEJ magnetic effects (dotted line) in Brazil during the IEEY.

where $I_0(t)$ is the current intensity at the EEJ center at a given hour (t) and I_{12} is the local noon value of $I_0(t)$ estimated by eq. (4).

The time function $I_0(t)$ can be combined with any of the latitudinal current distributions models (Eqs. (1)–(3)) to describe the latitudinal as well as local time dependence of the EEJ. If the quadratic distribution is adopted, the current function defining latitudinal and diurnal variation of the EEJ takes the form

$$I(x,t) = I_{12}\left(1 - \frac{(x-c)^2}{a^2}\right)^2 \exp\left(-\frac{(t-T)^2}{t_m^2}\right). \qquad (8)$$

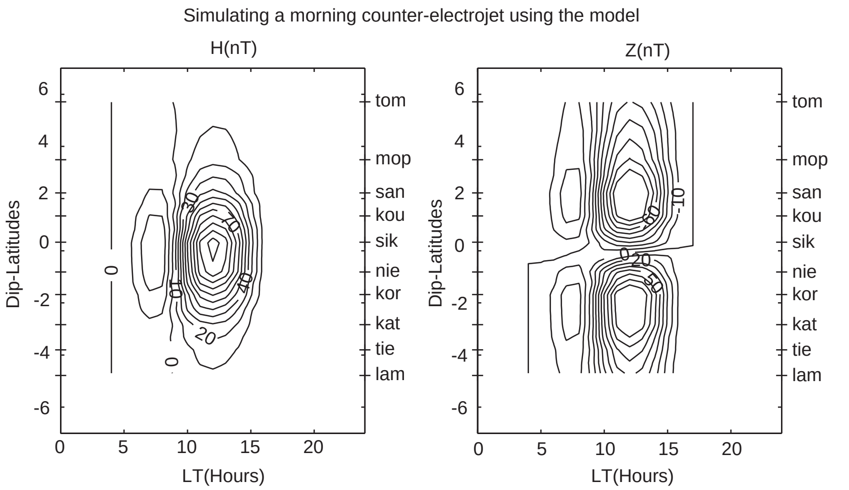

Fig. 4. Simulation of a morning counter-electrojet using the empirical model, under the assumption of a secondary ribbon flowing westward (with I_{0CEJ} corresponding to a $\Delta H = -30$ nT, and $T_{CEJ} = 8$ h LT and $t_m = 3$ h). I_{0CEJ} is the maximum intensity of the CEJ, T_{CEJ} is the local time the CEJ maximum intensity. The same half-width and position of the center axis were used as for the eastward EEJ.

In the present study, we use the quadratic current distribution because it satisfactorily accounts for the observed magnetic effects of the EEJ (Fambitakoye and Mayaud, 1976).

A distinctive feature of such a representation is that it can be used to simulate the counter-electrojet (CEJ) simply by assuming a secondary current ribbon flowing westward in addition to the normal eastward EEJ. In that case, the current intensity of the CEJ at the center is denoted by I_{0CEJ} corresponding to the time (T_{CEJ}) of the CEJ maximum intensity. Fig. 4 shows magnetic field variations associated with a morning counter-electrojet, as simulated by the model, where I_{0CEJ} corresponds to $\Delta H = -30$ nT, $T_{CEJ} = 8$ h LT and $t_m = 3$. From the dense network of stations across the dip-equator along the Indian sector, Arora et al. (1993) observed that latitudinal extent of the CEJ-related depression does not extend beyond the normal width of the EEJ. Given this evidence, the half-width (a) as well as h and c for the CEJ related ribbon were chosen to be same as for the normal EEJ, that is, $a = 330$ km, corresponding to the mean value of the EEJ half-width obtained by Doumouya et al. (1998).

2.3. Longitude dependence of the EEJ

The strength of the EEJ is best expressed by the current intensity at the EEJ center. This parameter is related to the ionospheric regular dynamo and in turn depends on the local magnitude of the main field through the ionospheric conductivity and is given by Ohm's law in the low-latitude ionosphere (Davis et al., 1967). Both the Pedersen conductivity (σ_1) and Hall conductivity (σ_2) depend on the intensity of the main field (B) through the gyro-frequency (Baker and Martyn, 1953). The longitudinal inequalities in the main field will induce longitudinal variation in the EEJ intensity.

In this section, the longitudinal dependence of the EEJ will be expressed by a numerical spline function estimated through surface measurements of ΔH along the dip-equator. To this end, we use available magnetic data recorded in different longitude sectors during the IEEY (Table 1). These data were recorded in three networks of magnetic stations: in West Africa ($\simeq$ 4.85°W), in Brazil ($\simeq$ 43.49°W) and in India ($\simeq$ 77.23°E). Three individual stations close to the dip-equator are added. These are Ancon (77.02°W, 1.47° dip-latitude) in Peru, Mokolo (13.48°E, −0.29° dip-latitude) in Cameroon and Yap Island (138.04°E, 0.71° dip-latitude) in the Pacific, providing a network of 26 stations (Fig. 5). For the longitude sectors where a chain of stations is available, ΔH at the center of the EEJ is given by the peak value in the latitudinal profiles of the horizontal field measured with respect to the field at local night. For the longitudinal sector represented by a single site, given their proximity to the dip equator, the station's ΔH is taken to be the measure of the EEJ intensity at the central axis. Since a reference station located outside of the influence of the electrojet is required to remove the planetary Sq contribution to the geomagnetic field at the dip equator, we decided not to eliminate the Sq contribution in order to keep the same baseline for the regular daily range.

Fig. 6 shows the mean values of ΔH along the central axis (dip-equator) of the EEJ at six different longitude sectors separately for various local times, from 9 LT to 15 LT. These averages are obtained on the data of 13 quiet days, selected on the basis of magnetic quiet conditions, ignoring seasonal criteria (Table 2). The error-bars represent the standard deviations. The solid line is obtained using spline interpolation. We perform this interpolation and set ΔH continuous across the 180° meridian, and in station-free sectors

Table 1

Stations	Code	Geographic		Dip Lat (°)
		(°N)	(°W)	
(a) *Geomagnetic stations operated during the IEEY in West Africa*				
Tombouctou	TOM	16.733	3.000	5.51
Mopti	MOP	14.508	4.087	3.29
San	SAN	13.237	4.879	2.02
Koutiala	KOU	12.356	5.448	1.13
Sikasso	SIK	11.344	5.706	0.12
Nielle	NIE	10.203	5.636	−1.01
Korhogo	KOR	9.336	5.427	−1.88
Katiola	KAT	8.183	5.044	−3.04
Tiebissou	TIE	7.218	5.241	−4.00
Lamto	LAM	6.233	5.017	−4.99

Observatory	Code	Geographic		Dip Lat (°)
		(°N)	(°E)	
(b) *Geomagnetic stations functioning during the IEEY in India*				
Ujjain	UJJ	23.18	75.78	18.42
Alibag	ABG	18.63	72.86	12.96
Hyderabad	HYD	17.42	78.55	11.16
Anantapur	ANT	14.67	77.63	7.83
Bangalore	BAN	12.98	77.60	5.72
Annamalainagar	ANN	11.37	79.68	3.67
Karur	KAR	11.01	78.09	3.32
Virudunagar	VIR	9.61	77.94	1.61
Trivandrum	TRD	8.48	76.95	0.28

Observatory	Code	Geographic		Dip Lat (°)
		(°N)	(°W)	
(c) *Geomagnetic stations operated during the IEEY in Brazil*				
Belem	BLM	−1.22	48.53	1.94
Sao Luis	SLZ	−2.60	44.20	0.95
Eusebio	EUS	−3.85	38.42	−0.81
Teresina	TER	−5.03	42.83	−0.54

(in the Pacific region), we add or subtract 360° from the real longitudes of the various locations.

The shape of the longitudinal profiles is roughly similar around noon hours. This shape is observed every day with some secondary day-to-day changes but the amplitude variations from one day to another are quite significant. Around noon, the amplitude (ΔH) is maximum in South America. It regularly decreases and shows an inflexion in Africa with a secondary maximum at about 10° longitude. It remains decreasing to a minimum in India and then increases regularly from India to South America with another inflexion in the West Pacific. Before 11 LT and after 14 LT, the shapes of the longitudinal profiles of ΔH show a very strong day-to-day variability. Before 11 LT, the profiles have two maxima, in Brazil and Central Africa (at Mokolo), and two minima, in West Africa and in India. The minimum in India is less pronounced at 9 LT. In fact, the shape before 11 LT does not fully vanish. For example, the maximum in South America and the minimum in India are more pronounced around noon and the maximum and the minimum in Africa are less marked.

The longitude dependence function of the model is empirically taken into account using a spline interpolation. In this section, the longitudinal dependence of the EEJ will be expressed by a numerical spline function estimated through surface measurements of ΔH along the dip-equator.

Fig. 7 presents the longitudinal dependence of the EEJ as expressed by the numerical spline function fitting the mean

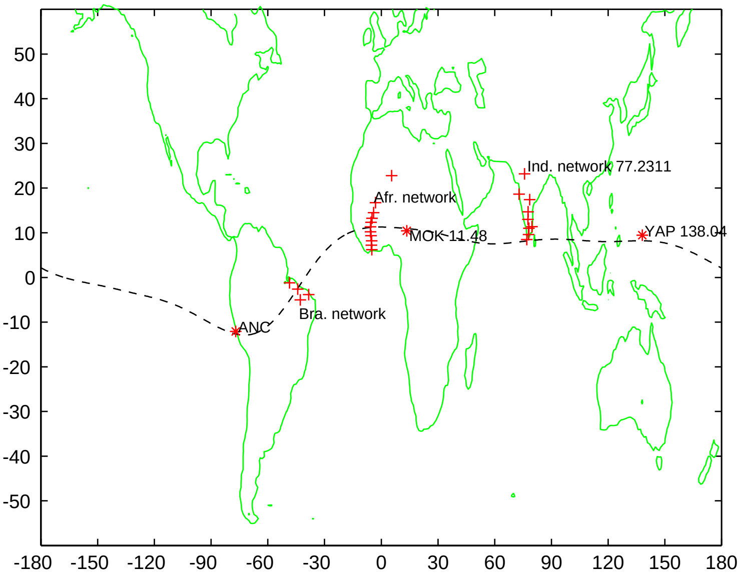

Fig. 5. Locations of the equatorial networks and stations whose magnetic measurements are used for the study of longitude dependence of the EEJ.

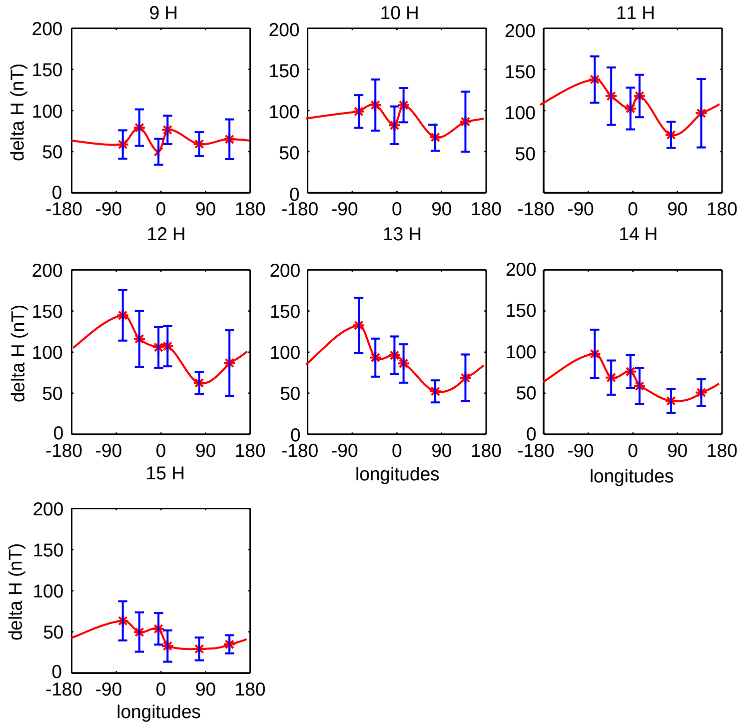

Fig. 6. The averaged longitude dependence of the magnetic effects of the equatorial electrojet, from 9 to 15 LT. The error bars represent the standard deviations of ΔH with respect to the averages of 13 days' data.

ΔH at 12 LT along the dip-equator, $I_{12}(\lambda)$. Also shown is the inverse of the main intensity field ($1/B$) at the dip-equator, multiplied by an arbitrary factor $5 \times 10^{+6}$ in order to reach the same amplitude range as ΔH. This figure shows an approximate inverse correlation between ΔH and the main field (B).

Table 2
Selected magnetically quiet days for the study of the longitude dependence of the EEJ

Selected quiet days	Brazilian network	African network	Indian network	Ancon (ANC)	Mokolo (MOK)	Yap Island (YAP)
23/02/1993	X	X	X	X	–	X
24/02/1993	X	X	X	X	–	X
25/02/1993	X	X	X	X	–	X
26/02/1993	X	X	X	X	–	X
05/03/1993	X	X	X	X	X	X
06/03/1993	X	X	X	X	X	X
26/04/1993	X	X	X	X	X	–
27/04/1993	X	X	X	X	X	–
28/04/1993	X	X	X	X	X	–
24/05/1993	X	X	X	X	X	X
25/05/1993	X	X	X	X	X	X
26/05/1993	X	X	X	X	X	X
15/06/1993	X	X	X	X	X	X

"X" indicates data availability at different locations and "–"indicates lack of data.

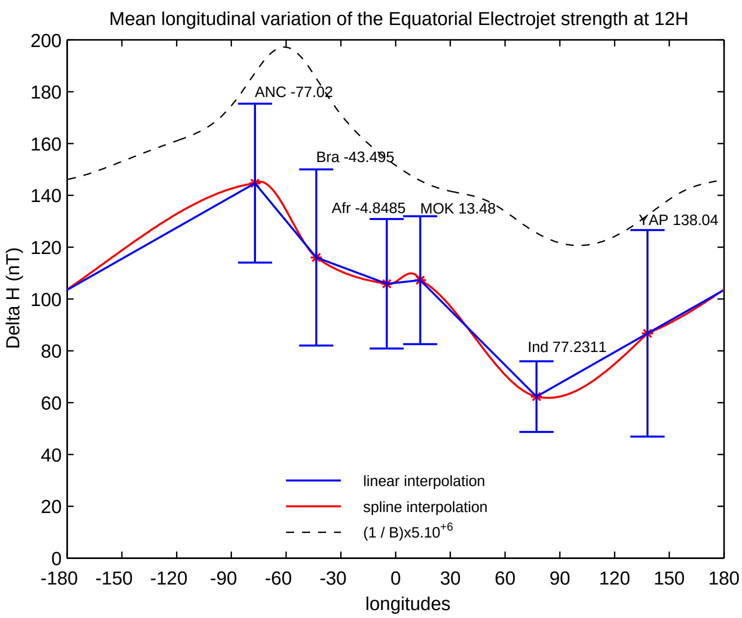

Fig. 7. The mean longitude dependence of the magnetic effects of the equatorial electrojet at 12 LT (solid curve) and the inverse of the main field $5 \times 10^6/B$ (dashed line). The error bars represent the standard deviations of ΔH with respect to the averages of 13 days data.

3. The empirical model of the EEJ and its validation

In the preceding section, three independent functions are defined to express the latitudinal (Eq. (3)), local time (Eq. (7)) and longitudinal, $I_{12}(\lambda)$, dependence of the EEJ. The product of these three functions, as expressed below, represents an empirical EEJ model that can effectively describe the spatial (latitudinal and longitudinal) and temporal characteristic of the electrojet currents

$$I(x,\lambda,t) = I_{12}(\lambda)\left(1 - \frac{(x-c)^2}{a^2}\right)^2 \exp\left(-\frac{(t-T)^2}{t_{\mathrm{m}}^2}\right). \tag{9}$$

Note that the local time (t) depends also on the longitudes at a given universal time (t_{u})

$$t = t_{\mathrm{u}} + \frac{\lambda}{15}, \quad -180^\circ < \lambda < 180^\circ.$$

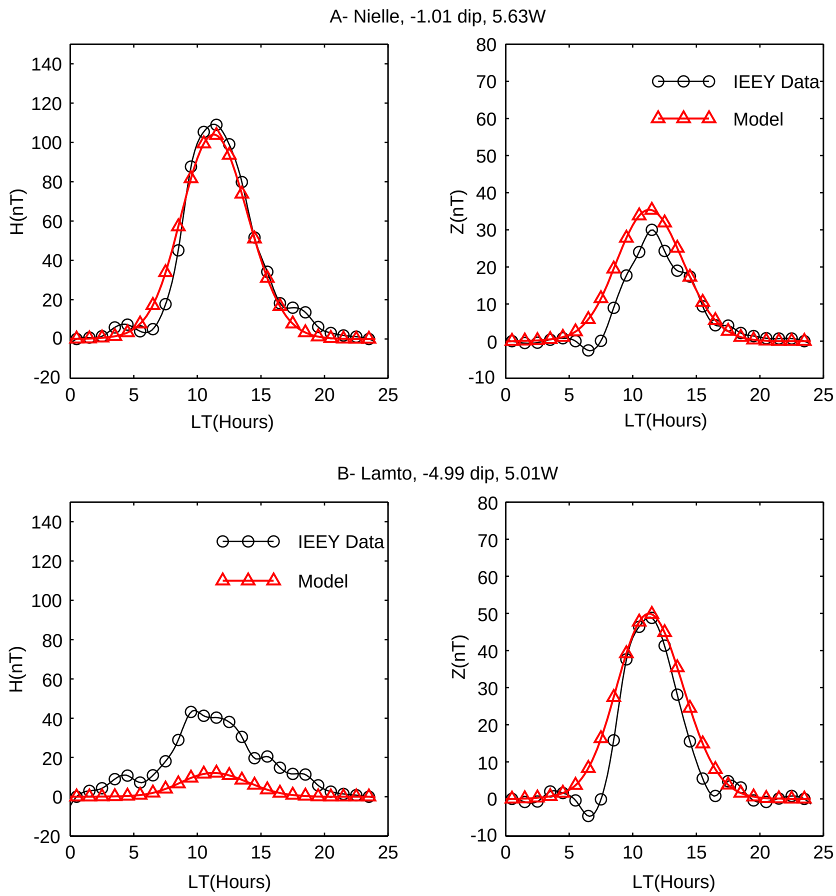

Fig. 8. Comparison between the observed and computed daily variation of H and Z components of the equatorial electrojet magnetic effects, February, 23rd 1993 at Nielle and Lamto.

Once the model parameters, c, a, T, t_m and $I_{12}(\lambda)$, are determined from the data, the following expressions, corresponding to the fourth degree current distribution (Fambitakoye, 1976), can be used to compute the magnetic fields in H and Z for a stations located at a given position xs;

$$H = 0.2\,\frac{I_0}{a^4}\,[(a^2 - X_S^2)^2 + (2a^2 - 6X_S^2)h^2 + h^4](\arctan R_B - \arctan R_A) + 0.2\,\frac{I_0}{a^4}\,[2(a^2 - X_S^2)X_S h + 2X_S h^3][\ln(1+R_B^2) - \ln(1+R_A^2)] + 0.2\,\frac{I_0}{a^4}\,\frac{h^4}{3}(R_B^3 - R_A^3) - 0.4\,\frac{I_0}{a^4}\,X_S h^3(R_B^2 - R_A^2) - 0.2\,\frac{I_0}{a^4}\,[(2a^2 - 6X_S^2)h^2 + h^4](R_B - R_A),$$

$$Z = -0.1\,\frac{I_0}{a^4}\,[(a^2 - X_S^2)^2 + (2a^2 - 6X_S^2)h^2 + h^4][\ln(1+R_B^2) - \ln(1+R_A^2)] + 0.8\,\frac{I_0}{a^4}\,[(a^2 - X_S^2)X_S h - X_S h^3](\arctan R_B - \arctan R_A) - 0.1\,\frac{I_0}{a^4}\,\frac{h^4}{2}(R_B^4 - R_A^4) + 0.8\,\frac{I_0}{a^4}\,\frac{h^3}{3}X_S(R_B^3 - R_A^3) + 0.1\,\frac{I_0}{a^4}\,[(2a^2 - 6X_S^2)h^2 + h^4](R_B^2 - R_A^2) - 0.8\,\frac{I_0}{a^4}\,X_S[(a^2 - X_S^2)h + h^3](R_B - R_A),$$

where

$$X_S = xs - c,$$

$$R_A = \frac{X_S - a}{h},$$

$$R_B = \frac{X_S + a}{h}$$

when c (the position of the EEJ center), a (the half-width) and h (the height of the EEJ) are in km; I_0 (the current intensity at the EEJ center) is in A/m, the H and Z are in nT. In the emperical model developed, I_0 is represented by the time and longitude varying current intensity I_{12} (t, λ) near the dip-equator (first and last tern in Eq. (9)), the model permits to study the characteristic variations of the EEJ with latitude, longitude, altitude and time.

3.1. Comparison with ground magnetic data on quiet days during IEEY

The magnetic daily variations of 40 quiet days were used as input to determine model parameters in eq. (8). These parameters are used to compute magnetic fields at the locations of the IEEY stations in West Africa and elsewhere. This approach thus allows a direct comparison between measured and modeled EEJ effects. Fig. 8 compares the observed daily variations in H and Z on February 23rd 1993 at the West African IEEY stations, Niellé ($-1.01°$ dip-latitude) and Lamto ($-4.99°$ dip-latitude), with those derived from the model. For this example $a = 331$ km, $\Delta H = 112.9$ nT ($I_{12} = 223.3$ A/m) and $c = 10.99°$N. It is seen that the patterns of measured and modeled daily variation of the EEJ are quite similar and their magnitudes at Niellé in the course of day are within 10 nT or an accuracy of about 9%. At the station Lamto there is an extreme case of misfit. Differences between data and model are quite large, reaching 36 nT (32%) in ΔH around noon.

Fig. 9 shows the latitudinal profile of the ΔH and ΔZ at different local times as recorded on March, 5th 1993 along the West African sector together with model computed fields, for $a = 317$ km, $\Delta H = 118.3$ nT ($I_{12} = 236.3$ A/m) and $c = 10.92°$N. These profiles are roughly similar. The amplitudes of the H component are comparable near the dip-equator, where the differences between data and modeled ΔH are less than 20 nT (17%) between 9:30 and 14:30. Near the fringe latitudes of the EEJ, the differences are about 35 nT (30%). For the Z component, the differences are more pronounced near the maximum and the minimum (about ± 30 nT) in the latitudinal profile for noon, and less elsewhere. The contour plots of the ΔH and ΔZ fields in the latitudinal-local time frame (Fig. 10) exhibit an overall agreement between observed and modeled components. Small differences in shapes, both in H and Z, may arise from the fact that the current model is designed to be perfectly symmetrical with respect to the dip-equator as well as to local noon. The nature of disagreement becomes more conspicuous in Fig. 11 where the differences between measured and modeled ΔH during four consecutive quiet days in February 1993 are shown in the form of contour maps. These contour maps display a negative zone in the morning (5:00 to 10:00) with a minimum at about 8:00. The presence of this well developed low on these selected days appears to be related to the occurrence of a CEJ.

Doumouya et al. (1998) have classified the selected quiet days during the IEEY as counter-electrojet days and non-counter-electrojet days. February 25–26, 1993, were identified as days of morning counter electrojet (CEJm) in the West African sectors and the daily variations in H were marked by a negative excursion in the morning hours, going down well below the nighttime level. The strong negative anomaly pattern, reaching an amplitude of -50 nT on February 25–26, 1993 (Fig. 11b) could be attributed to the occurrence of morning CEJ. Similarly, the weak negative low of -15 nT seen on February 23–24 might mark the presence of a partial counter electrojet. Since the negative excursion associated with a CEJ in the equatorial belt at certain times is accompanied by a perturbation at low and mid latitudes (Stening, 1977; Arora et al., 1993), the strong positive residual field observed near the edge of the electrojet (Fig. 11b) might again be related to CEJ occurrence. But more detailed future work is necessary to emphasize these features.

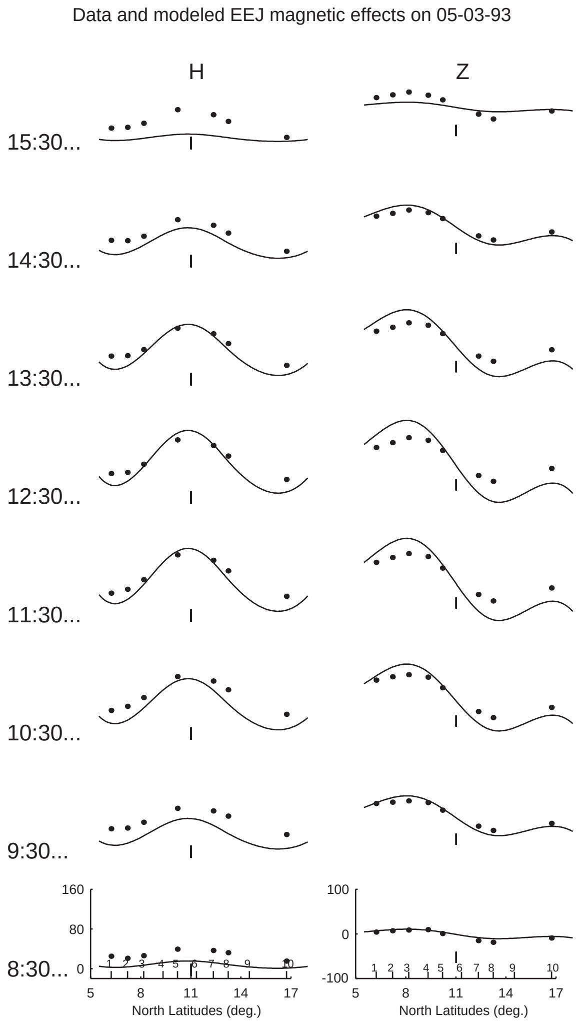

Fig. 9. Comparison between the observed (dots) and computed latitudinal variation (solid lines) of H and Z components of the equatorial electrojet magnetic effects. The vertical line below each curve indicates the position of the dip-equator.

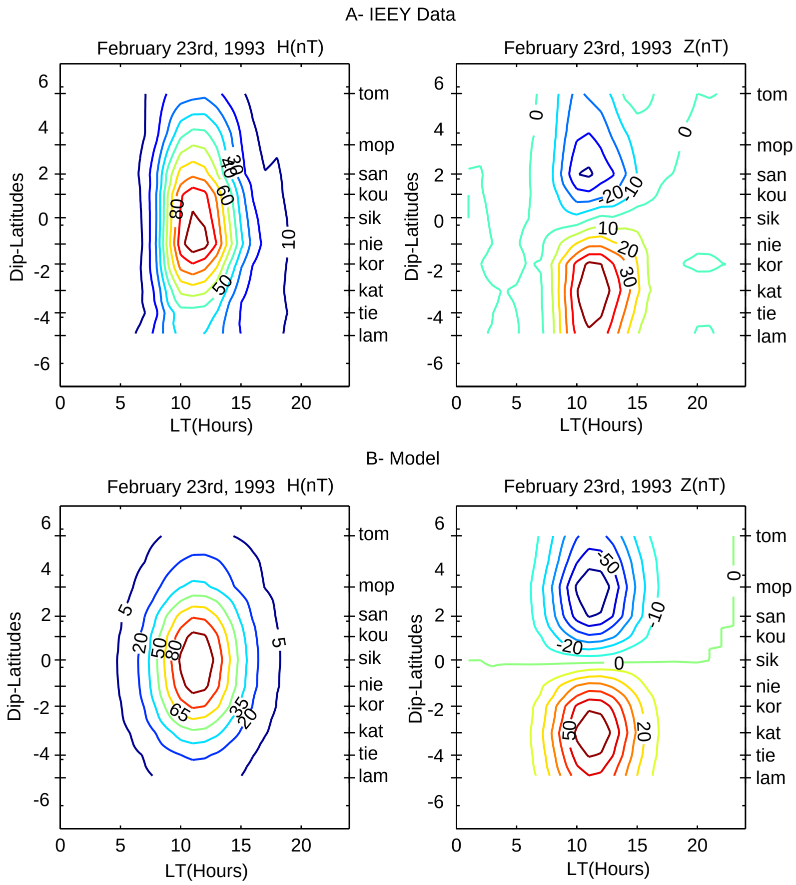

Fig. 10. Contour maps of observed and computed daily variation of the H and Z components of the equatorial electrojet magnetic effects.

It can be summarized that the empirical model reproduces the average magnetic signatures of the EEJ on a global scale, though it might not be the right choice for detailed analysis of day-to-day variability, especially days of CEJ occurrence. However, it is shown that if model parameters are determined including CEJ conditions, the model can simulate the negative surface magnetic fields.

3.2. *Comparison with POGS satellite EEJ magnetic signature above the IEEY network in West Africa*

The numerical formulation adopted allows computation of the magnetic effects at any altitude (Eq. (4)). Fig. 12 gives, both in contour form as well as perspective view, the model simulated ΔH and ΔF at an altitude of 700 km. In such a simulation, the EEJ is assigned a half-width of 330 km and its intensity corresponds to a ground ΔH of 100 nT. At this height the EEJ effects are expectedly weaker (Fig. 12a) than that observed at ground level (Fig. 10b), and the shape of the latitudinal profile of the EEJ signature is reversed. Also, as expected, the magnetic fields have a much wider latitudinal extent. In order to validate the extent to which the model parameters determined from simultaneous ground-based measurement can reproduce variations at satellite heights, we have compared model estimated magnetic effects with those measured on board the POGS satellite, the only satellite that was operational during the IEEY. In Fig. 13, we present latitudinal plots of the modeled ΔF (residual total field) and that recorded on board the POGS satellite on different days while transiting the longitude band $\pm 15°$E, i.e. centered along the West African IEEY network.

Assuming that the EEJ signature is restricted to a latitude band of $\pm 30°$, we isolate the EEJ signature removing longer wavelength variations. These examples show that, on passes when characteristic EEJ signatures are seen in POGS magnetic data, e.g. on July 2, 13 and 21, 1993, the model amplitude of the EEJ compares favorably with observations. However, on certain passes (June 21, 29, 1993 and July 29, 1993) the discrepancies between the observations and the model are quite large. Since on such passes the observed magnitudes and spatial structures are highly modulated, it

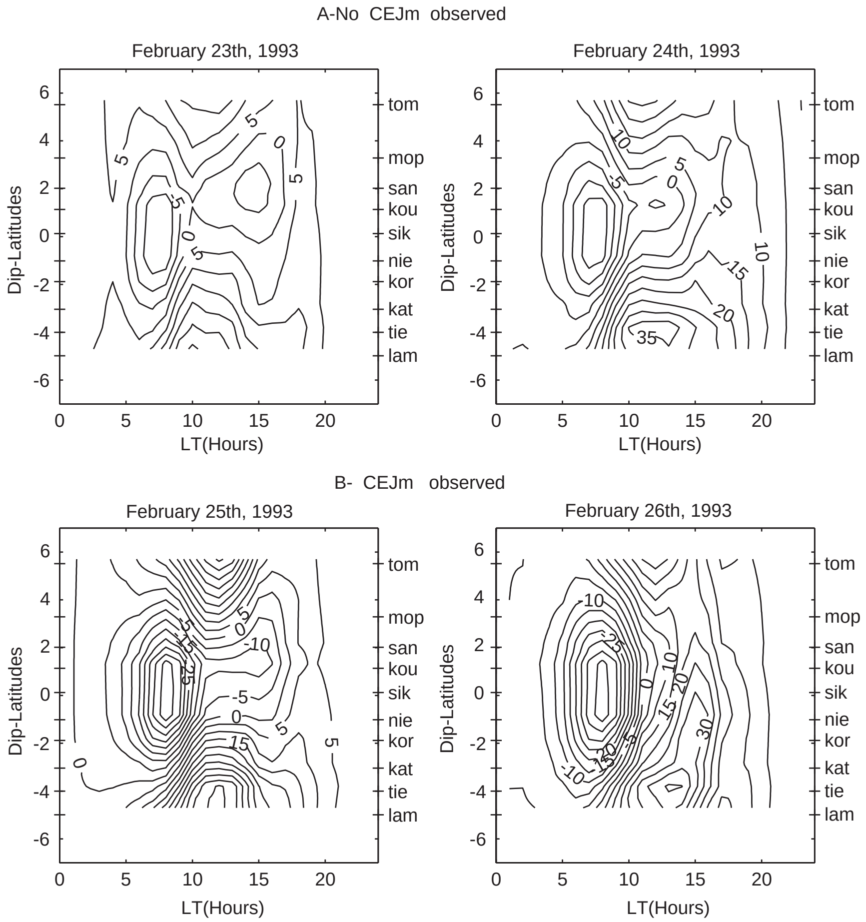

Fig. 11. Contour maps of the difference between observed and computed daily variations of the H component of the magnetic effects of the equatorial electrojet.

is likely that there is a contribution from sources other than the electrojet.

4. Discussion

An empirical EEJ model has been proposed that can be used to describe the nature of the associated magnetic fields with local time, latitude and longitude as well as with height. One of the novel features of the proposed empirical model is that it incorporates a dependence on longitude. It is the first time that the longitudinal dependence of the EEJ magnetic effects has been studied using simultaneous surface data sets in six longitude sectors (three extended networks of stations and three individual stations).

The longitudinal variation in the strength of the EEJ, defined by $I_0(\lambda)$ in Eq. (9) and shown in Fig. 7, is consistent with previous studies of the longitudinal dependence obtained from POGO satellite data (Cain and Sweeney, 1973) as well as from Magsat dusk data (Ravat and Hinze, 1993). However, the present results show only partial agreement with the longitudinal inequalities in the EEJ current density and total current intensity deduced from using the POGO satellite data (Onwumechili and Agu, 1980). More recently, Kim and King (1999) have revisited the POGO data to establish the true nature of the longitudinal variation in the EEJ. They found longitudinal inequalities obtained utilizing POGO passes scanning all altitude ranges to be very different in comparison with those when only passes below 450 km altitude were employed. The cause of this discrepancy remains unknown and further investigations were suggested. Despite the wide separation between the successive chains of stations and the absence of stations in the Pacific, the agreement between our present results and those obtained from POGO and Magsat suggests that weak longitudinal gradients in EEJ magnetic signatures minimize the errors in the longitudinal interpolation of the field from a widely distributed set of stations. The plots of longitudinal

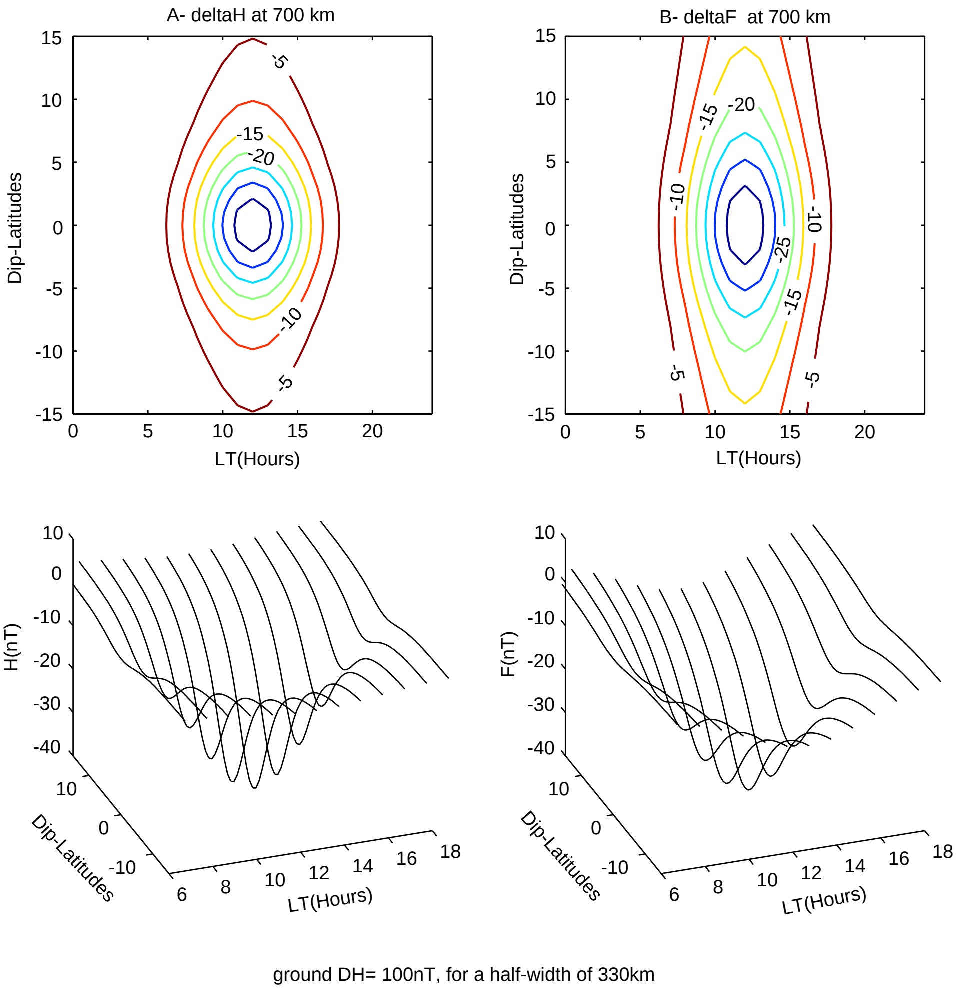

Fig. 12. Simulated magnetic effects of the equatorial electrojet at 700 km altitude, for an EEJ ground ΔH of 100 nT and half-width of 330 km: (a) ΔH and (b) ΔF.

inequality in the EEJ strength (Fig. 7) clearly bring out the inverse correlation with the main magnetic field strength, an inference drawn earlier from restricted longitudinal sets of data (Rastogi, 1962).

5. Applications of the empirical model

The other salient merit of the empirical model is that EEJ parameters determined from surface measurements can be used to estimate the magnetic field directly at satellite heights and this can be exploited to seek the relationship between surface and satellite magnetic signatures of the EEJ. This problem has been addressed by various workers using the POGO data (Cain and Sweeney, 1973; Osborne, 1973; Ebun Oni, 1973; Yacob and Bhargava, 1973, Kane, 1973; Gouin, 1973; Agu and Onwumechili, 1981). Agu and Onwumechili (1981) have shown a linear correlation between surface and satellite EEJ magnetic signatures. The inclusion of the local time and longitudinal dependence terms in the present model should prove effective in extrapolating the magnetic signature of the EEJ at satellite altitude to different longitudes and local times. This is a basic pre-requisite as non-sun-synchronous satellites sweep all longitudes and cross the EEJ at different local times. Once the validity of the scheme to extrapolate the surface magnetic field to satellite heights is established, the computed fields can be used for various applications such as:

1. Validating the EEJ models determined from the magnetic measurement on board satellites.
2. Correcting satellite/aeromagnetic magnetic field measurements for EEJ contamination when estimating a crustal magnetic anomaly.

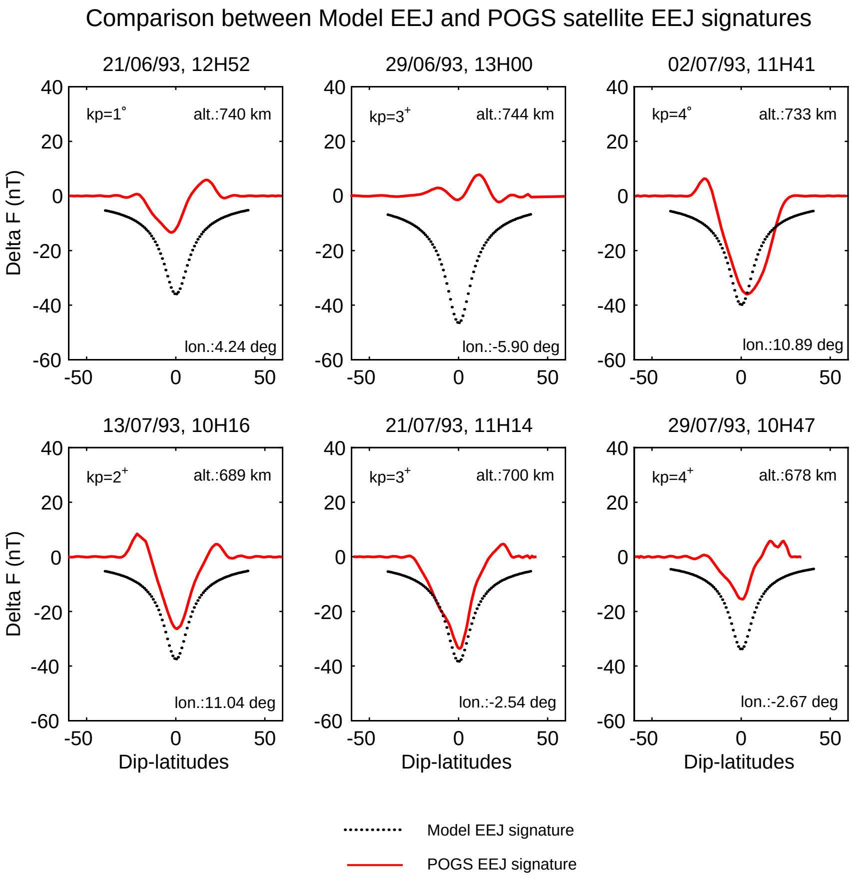

Fig. 13. Comparison between the POGS magnetic signature of the EEJ and the model. The modeled curves are computed using parameters derived from surface measurements.

3. Estimating the residual effects of the EEJ on a model of the main field derived from satellite magnetic data.

While the model in general produces the expected amplitude and spatial characteristics of the EEJ at satellite altitudes, the comparison of observed and model response at satellite heights revealed large differences on certain individual passes. Thus the validation of the satellite-derived EEJ model, obtained by projecting surface magnetic data to the satellite height (item 1 above), could be achieved only in a statistical sense where data are averaged over a large number of passes. Under items 2 and 3, conventionally the data from a large number of passes are combined and hence the effects of day-to-day variability, from both EEJ and magnetospheric sources, may be averaged out. Therefore, the EEJ model parameters obtained from surface magnetic data could be used to estimate and eliminate the overall contribution of the EEJ from the satellite data.

Fig. 14a shows the global view of the horizontal and vertical components of the magnetic signature of the EEJ at a given universal time (10 UT) at 450-km altitude. The magnetic fields in the equatorial belt have been obtained substituting the mean longitudinal profile of ΔH at 12 LT in the empirical model represented (Fig. 7). For this computation, the position of the dip-equator has been considered as the EEJ center and a constant half width of 330 km has been used. Fig. 14b shows the sun-synchronous view of the horizontal and vertical components of the magnetic signature of the EEJ at 12 LT. This figure is obtained after sweeping all universal time from 0 to 24 UT.

6. Conclusions

The current distribution models used to describe the latitudinal structure of the EEJ are reviewed. An empirical model of the EEJ involving longitude, latitude and local time dependence has been proposed. We showed that the local time dependence of the EEJ signature is well described by an empirical gaussian-like function near the EEJ center. The model was tested using surface data as well as POGS

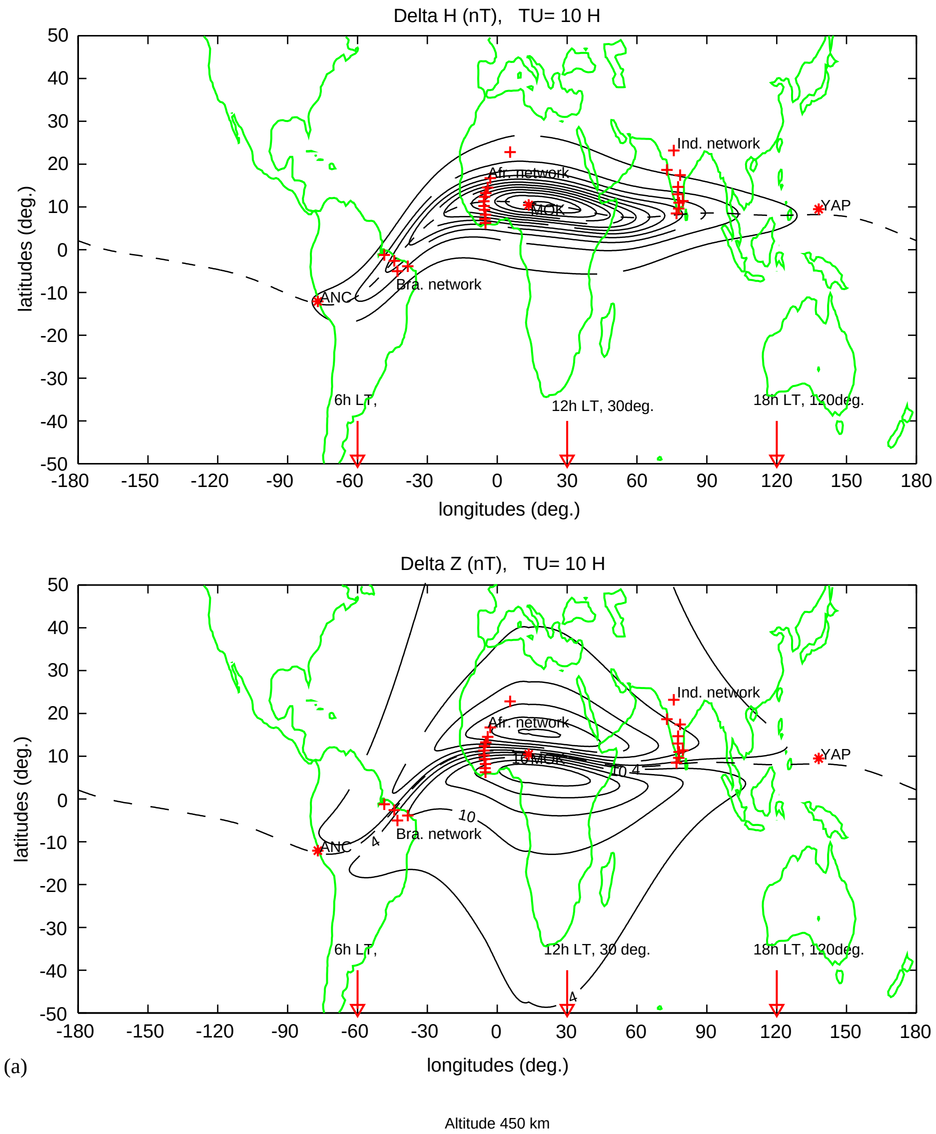

Fig. 14. (a) Global view of the H and Z components of the EEJ magnetic effects at a fixed universal time (10 UT) at an altitude of 450 km. ΔH contour interval is 5 nT for a minimum of about -60 nT, ΔZ contour interval is 6 nT for a minimum of about -30 nT and a maximum of 30 nT; (b) sun-synchronous view of the H and Z components of the EEJ magnetic effects at a fixed local time (12 LT) at an altitude of 450 km. ΔH contour interval is 10 nT for a minimum which depends on the longitude, it is about -50 nT in Africa, -70 nT in South America and -30 nT in India. ΔZ contour interval is 10 nT for a minimum of about -30 nT and a maximum of 30 nT in Africa.

satellite data. These results showed that the model determined from ground-based EEJ measurements describes well the magnetic signature of the EEJ on the ground with errors less than 17% around noon and near the dip-equator, whereas large discrepancies are sometimes observed between modeled and satellite EEJ signatures. Such discrepancies might be due to many causes. First, one might think of magnetospheric current systems, especially field-aligned currents whose effects could be stronger at satellite altitudes. Altitude changes of about 70 km along a single satellite pass are possible. That would affect the determination of the EEJ signature and could be one of the sources of the observed discrepancies. POGS provided only scalar magnetic data. Vector and scalar magnetic measurements from the Oersted and CHAMP satellites, which fly at lower altitudes, will be used for a wider comparative study. The CHAMP satellite could provide a better estimation of the EEJ magnetic signatures because of its lower altitude.

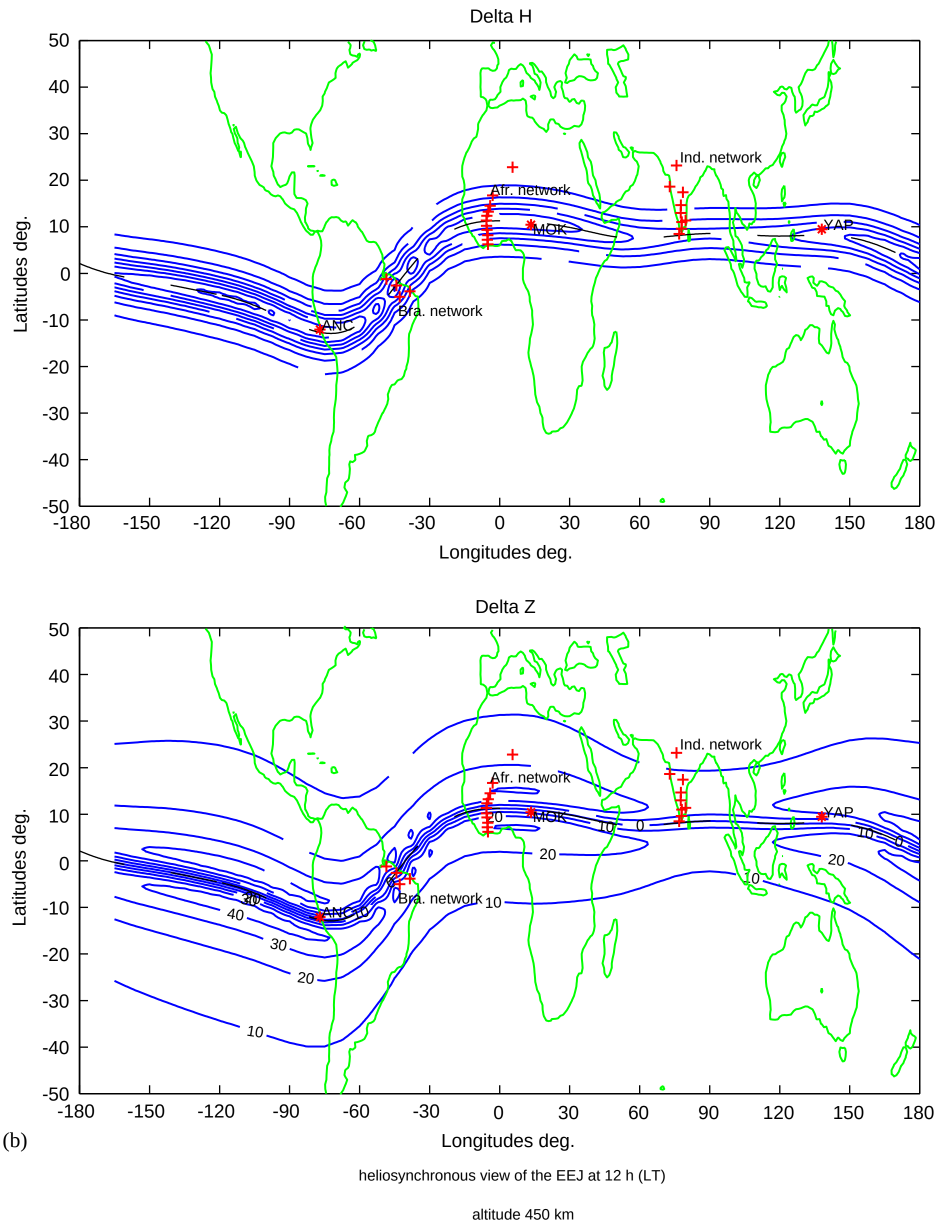

Fig. 14. *continued.*

In this work, the longitudinal dependence of the EEJ is numerical represented for the first time from simultaneous surface magnetic records in different longitude sectors. This study showed that the magnetic signature of the EEJ is stronger in South America with a maximum between 80° and 100°W. An inflexion, with sometimes a secondary minimum observed in the Atlantic Ocean (30°W), is followed by a secondary maximum in West Africa at about 0°E. The EEJ magnetic signature is weaker in Asia, with a minimum in India, between 75° and 100°E. A weak inflexion is also observed in the Pacific Ocean at about 140°E. These longitude variations of the EEJ magnetic effect roughly follow variations of the inverse main field ($1/B$) at the dip equator.

Acknowledgements

We gratefully thank all the people who provided us with all the data used in this worldwide compilation. We also thank French research Institutes IRD (Institut pour la Recherche et le Developpement) and INSU (Institut National des Sciences de l'Univers) for the support in west Africa. Dr. Doumouya Vafi was supported by the French Ministère de la Cooperation for his stays in France. Authors wish to thank Robert Stening and K.N. Iyer for their constructive comments.

References

Agu, C.E., Onwumechili, C.A., 1981. Comparison of the POGO satellite and ground measurements of the magnetic field of the equatorial electrojet. Journal of Atmospheric and Terrestrial Physics 43, 801–807.

Amory-Mazaudier, C., Vila, P., Achache, J., Achy Séka, A., Albouy, Y., Blanc, E., Boka, K., Bouvet, J., Cohen, Y., Dukhan, M., Doumouya, V., Fambitakoye, O., Gendrin, R., Goutelard, C., Hamoudi, M., Hanbaba, R., Hougninou, E., Huc, C., Kakou, K., Kobea-Toka, A., Lassudrie-Duchesne, P., Mbipom, E., Menvielle, M., Ogunade, S.O., Onwumechili, C.A., Oyinloye, J.A., Rees, D., Richmond, A., Sambou, E., Schmuker, E., Tirefort, J.L., Vassal, J., 1993. International equatorial electrojet year: the African sector. Revista Brasileira de Geofisica 11, 303–317 (Especial).

Arora, B.R., Mahashabde, M.V., Kalra, R., 1993. Indian IEEY geomagnetic observational program and some preliminary results. Brazilian Journal of Geophysics 11 (3), 365–384.

Baker, W.G., Martyn, D.F., 1953. Electric current in the ionosphere, I—The conductivity. Philosophical Transactions of Royal Society of London A 245, 251–294.

Cain, J.C., Sweeney, R.E., 1973. The POGO data. Journal of Atmospheric and Terrestrial Physics 35, 1231–1247.

Chapman, S., 1951. The equatorial electrojet as detected from the abnormal electric current distribution above Huancayo, Peru and elsewhere. Archiv fuer Meteorologie, Geophysic und Bioclimatologie, Series A 44, 368–390.

Chapman, S., Bartels, J., 1940. Geomagnetism. Clarendon Press, Oxford.

Cohen, Y., Achache, J., 1990. New global vector anomaly maps derived from MAGSAT data. Journal of Geophysical Research 95, 10783–10800.

Davis, T.N., Burrows, K., Stolarik, J.P., 1967. A latitude survey of the equatorial electrojet with rocket-borne magnetometers. Journal of Geophysical Research 72, 1845–1861.

Doumouya, V., Vassal, J., Cohen, Y., Fambitakoye, O., Menvielle, M., 1998. The equatorial electrojet: first results from magnetic measurement. Annales de Geophysicae 16, 658–676.

Ebun Oni, 1973. On the correlation of ground data at Ibadan with POGO satellite results. Journal of Atmospheric and Terrestrial Physics 35, 1267–1271.

Fambitakoye, O., 1976. Etude des effets magnetiques de l'electrojet equatorial (unpublished doctorate thesis). Service de Géophysique 14, ORSTOM.

Fambitakoye, O., Mayaud, P.N., 1976. The equatorial electrojet and regular daily variation S_R:—I. A determination of the equatorial electrojet parameters. Journal of Atmospheric and Terrestrial Physics 38, 1–17.

Forbush, S.E., Casaverde, M., 1961. The Equatorial Electrojet in Peru. Carnegie Institute Washington, Publ. 620.

Gouin, P., 1973. Correlation of 'satellite estimates of the equatorial electrojet intensity with ground observations at Addis Ababa. Journal of Atmospheric and Terrestrial Physics 35, 1257–1264.

Kane, R.P., 1973. Comparison of geomagnetic changes in India and the POGO data. Journal of Atmospheric and Terrestrial Physics 35, 1249–1252.

Kim, H.R., King, S.D., 1999. A study of local time and longitudinal variability of the amplitude of the equatorial electrojet observed in POGO satellite data. Earth Planets Space 51, 373–381.

Langel, R.A., Schnetzler, C.C., Philips, J.D., Horner, R.J., 1982. Initial vector magnetic anomaly map from Magsat. Geophysical Research Letters 9, 273–276.

Langel, R.A., Purucker, M.M., Rajaram, M., 1993. The equatorial electrojet and associated currents as seen in MAGSAT data. Journal of Atmospheric and Terrestrial Physics 55, 1233–1269.

Maeda, H., Iyemori, T., Araki, T., Kamie, T., 1982. New evidence of meridional current system in the equatorial ionosphere. Geophysical Research Letters 9, 243–245.

Maynard, N.C., 1967. Measurement of ionospheric currents off the coast of Peru. Journal of Geophysical Research 72, 1863–1875.

Onwumechili, C.A., 1967. Geomagnetic variations in the equatorial zone. Physics of Geomagnetic Phenomena—I. Academic Press, New York, London, pp. 425–507.

Onwumechili, C.A., 1992. Study of the return current of equatorial electrojet. Journal of Geomagnetism and Geoelectricity 44, 1–42.

Onwumechili, C.A., Agu, C.E., 1980. Longitudinal variation of the equatorial electrojet parameters derived from POGO satellite observations. Planetary Space Science 29, 627–634.

Osborne, D.G., 1973. Electrojet measurement from satellite and ground. Journal of Atmospheric and Terrestrial Physics 35, 1273–1279.

Rastogi, R.G., 1962. Longitudinal variation in the equatorial electrojet. Journal of Atmospheric and Terrestrial Physics 24, 1031–1040.

Ravat, D., Hinze, W.J., 1993. Consideration of variations in ionospheric field effects in mapping equatorial lithospheric Magsat magnetic anomalies. Geophysical Journal International 113, 387–398.

Reddy, C.A., 1989. The equatorial electrojet. Pure and Applied Geophysiscs 131, 485–508.

Richmond, A.D., 1973. Equatorial electrojet—I. Development of a model including winds and electric field. Journal of Atmospheric and Terrestrial Physics 35, 1083–1103.

Rigoti, A., Chamalaun, F.H., Trivedi, N.B., Padilha, A.L., 1999. Characteristics of the equatorial electrojet determined from an array of magnetometers in N–NE Brazil. Earth Planet Space 51, 115–128.

Sampath, S., Sastry, T.S.G., 1979. Results from in situ measurements of ionospheric currents in the equatorial region. Journal of Geomagnetism and Geoelectricity 31, 373–379.

Stening, R.J., 1977. Magnetic variations at other latitudes during reverse equatorial electrojet. Journal of Atmospheric and Terrestrial Physics 39, 1071–1077.

Stening, R.J., 1985. Modeling the equatorial electrojet. Journal of Geophysical Research 90, 1705–1719.

Sugiura, M., Cain, J.C., 1966. A model equatorial electrojet. Journal of Geophysical Research 71.

Sugiura, M., Poros, D.J., 1969. An improved model equatorial electrojet with meridional current system. Journal of Geophysical Research 74, 4025–4034.

Untiedt, J., 1967. A model of the equatorial electrojet involving meridional current. Journal of Geophysical Research 72, 5799–5810.

Vassal, J., Menvielle, M., Cohen, Y., Dukhan, M., Doumouya, V., Boka, K., Fambitakoye, O., 1998. A study of transient variations in the Earth's electromagnetic field at equatorial electrojet latitudes in western Africa (Mali and the Ivory Coast). Annales Geophysicae 16, 677–697.

Yacob, A., Bhargava, B.N., 1973. The electrojet field from satellite and surface observations in the Indian equatorial region. Journal of Atmospheric and Terrestrial Physics 35, 1253–1255.

Yanagisawa, M., Kono, M., 1985. Mean ionospheric field correction for Magsat data. Journal of Geophysical Research 90 (B3), 2527–2536.